

Central Exclusive Hadron Production in CDF

The CDF Collaboration

URL <http://www-cdf.fnal.gov>

(Dated: July 8, 2014)

Abstract

We present a study in CDF of $p\bar{p}$ collisions at the Tevatron that have two charged hadrons in the central region, $|\eta| < 1.3$ with large rapidity gaps (no hadrons) on either side. The reaction is $p + \bar{p} \rightarrow p + X + \bar{p}$, where the “+” stands for a rapidity gap G ; we use the notation GXG . Here we present a study of events with exactly two charged hadron tracks in the central detector, which we show to be often the result of the decay of a single neutral resonance, such as f_0^0 or f_2^0 states, or (rarely) the χ_{c0} . These events are expected to be dominated by double pomeron, \mathbb{P} , exchange in the t -channel; hence $\mathbb{P}+\mathbb{P} \rightarrow X$. Only specific quantum numbers for X are allowed. Additionally, we see a signal for photoproduction of the J/ψ state, which provides a check of our mass scale, resolution, and cross section calculation. We also place limits on exclusive production of χ_{c0} production and decay in the $\pi^+\pi^-$ and K^+K^- channels. We use data taken at $\sqrt{s} = 1960$ GeV and 900 GeV. This data provides a useful window on hadron spectroscopy, as well as providing benchmarks for testing pomeron models.

Preliminary Results for Summer 2014 Conferences

I. INTRODUCTION

The pomeron, \mathbb{P} , can be defined as the carrier of 4-momentum between protons when they scatter elastically at high (i.e. collider) energies. It is therefore a strongly interacting color singlet state, at leading order a pair of gluons: $\mathbb{P} = gg$. Of course in QCD it cannot be a pure state, because quark pairs and other gluons must evolve in when Q^2 , which we can equate with the 4-momentum transfer² t , becomes large. When Q^2 is small ($\lesssim 2 \text{ GeV}^2$) which is usually the case with pomeron exchange, perturbative QCD cannot be used to calculate cross sections, as the coupling $\alpha_s(Q^2)$ becomes of order 1. Non-perturbative methods, such as Regge theory, are more applicable. Here we study events in which pomerons from each incoming proton interact and create a pair of charged pions, a process called “double pomeron exchange” or DPE. The reaction is $p + \bar{p} \rightarrow p(*) + \pi^+\pi^- + \bar{p}(*)$ where the “+” denote large rapidity gaps with no hadrons. We do not detect outgoing $p(\bar{p})$ and they may dissociate (fragment) into low mass states ($p*$) as long as all the dissociation products (e.g. $p\pi^+\pi^-$, etc) have $|\eta| > 5.9$, the limit of the CDF detector. The pions have $|\eta(\pi)| < 1.3$, and with rapidity gaps on each side $\Delta\eta > 4.6$ DPE dominates, and the central $\pi^+\pi^-$ state must have $I^G J^{PC} = 0^+(\text{even})^{++}$ which is valuable quantum number filter for meson spectroscopy. Also, states with high glue content are favored, unlike in $\gamma\gamma \rightarrow X$ which favors $q\bar{q}$ states.

The CDF detector is described in detail in [1]. We only use events with no pile-up, where the full CDF detector with $-5.9 < \eta < +5.9$ is empty (noise levels) except for two charged tracks measured in the central tracker. The trigger requires at least two central calorimeter towers (EM + HAD) with $|\eta| < 1.3$ with a veto on BSC1 ($5.4 < |\eta| < 5.9$), CLC ($3.75 < |\eta| < 4.75$), and Forward Plug Calorimeter ($2.11 < |\eta| < 3.64$). The trigger was activated when the mean pile-up μ was low, e.g. at the end of stores. We took data at $\sqrt{s} = 1960 \text{ GeV}$, and during special low- s runs at $\sqrt{s} = 900 \text{ GeV}$ (about 40 hours in September 2011). The beam proton rapidities at the two \sqrt{s} values are $y_{beam} = \ln(\sqrt{s}/m(p)) = 6.87$ and 7.64 respectively. The “rapidity space” available for proton dissociation products is approximately (mixing true and pseudo-rapidities) $\Delta y(\text{diss}) = y_{beam} - 5.9 \sim 1.0$ and 1.74 respectively. The higher dissociation masses allowed at 1960 GeV than at 900 GeV will contribute to a higher measured cross section, and affect the quantum number selection rules; this should be borne in mind when studying the s -dependence of the cross sections.

The “exclusive efficiency” is the probability that a true event is not spoiled by another interaction. We measure this using a sample of zero-bias (bunch crossing with no other requirement) events, divided into two subsets: “interaction (with tracks etc.)” and “no-interaction” (no tracks or muon stubs) dominated. Plots of the energy or ADC counts in each subdetector determine where to put cuts defining “noise” or “activity”. Thus defining an empty detector over $|\eta| < 5.9$ we plot the probability $P(0)$ of an empty detector vs the individual bunch luminosities $L(\text{bunch})$, which is an exponential $P(0) = e^{-L(\text{bunch}) \times \sigma(\text{vis})}$, where $\sigma(\text{vis})$ is the cross section for events with any particles in $|\eta| < 5.9$. We estimate it from the total inelastic cross section $\sigma(\text{inel})$, from global fits [8] to $\sigma(\text{tot})$ and $\sigma(\text{elastic})$, correcting for the “invisible” part of the inelastic cross section, essentially only low-mass diffraction, from event Monte Carlo CDFSIM and PYTHIA [2]. At $\sqrt{s} = 1960$ GeV the delivered luminosity is known to $\pm 6\%$ using the CLC counters, and the exclusive efficiency is obtained from the distribution of bunch luminosities in the data weighted by $P(0) \cdot L(\text{bunch})$. At $\sqrt{s} = 900$ GeV the CLC counters were not calibrated, and we used $\sigma(\text{vis})$ to calibrate the overall luminosity. Applying the $\sigma(\text{vis})$ method at 1960 GeV gave agreement with the standard CLC method with a factor 1.04, within the overall uncertainty. The systematic uncertainty on the 900 GeV luminosity comes from the uncertainty on $\sigma(\text{vis})$ and on the slope of $P(0)$ vs $L(\text{bunch})$, and is 10%. The intercept of the $P(0)$ vs $L(\text{bunch})$ plot is > 0.99 , showing that at zero luminosity the probability of any hit above the noise cuts is $< 1\%$.

For the Gap-X-Gap triggered data, the events were cleaned up off-line by requiring all the CDF detectors to be “in the noise” apart from exactly two opposite charge tracks and the calorimeter towers to which they extrapolate.

We use the higher statistics 1960 GeV data to define the track cuts, and apply the same cuts at 900 GeV. We define the central region (i.e. region for reconstructed tracks) to be in $|\eta| < 1.3$, where the trigger was active. An opening angle cut, as well as the requirement of zero muons, eliminate the small background from cosmic ray tracks with $\theta_{3D} = \pi$. The track quality cuts consists of:

- Impact parameter to the nominal beam line cut, $d_0 < 0.1$ mm,
- The difference in z projected to the beam line $|dz_0| < 1.0$ cm,
- The number of COT hits in axial layers ≥ 25 ,

- The number of COT hits in stereo layers ≥ 25 ,
- $\chi^2/\text{DoF} < 2.5$.

To have a well-defined fiducial region and avoid rapidly changing thresholds we require both tracks to have $P_t > 0.4$ GeV/c. Additionally to be able to calculate the proper acceptance, we require that extrapolated tracks match two of the trigger towers with ± 1 tower tolerance in η and ϕ , and the rapidity of the two-track state to be $|y(\pi^+\pi^-)| < 1.0$.

Table I shows the numbers of events at several stages of the analysis, and the effective luminosity, at the two \sqrt{s} -values.

$\sqrt{s} =$	1960 GeV	900 GeV
Triggered events	90230×10^3	21737×10^3
After Forward exclusivity cuts	59538×10^3	18749×10^3
Exactly 2 tracks	4721×10^3	271×10^3
Quality, exclusivity, cosmic rejection	137128	6646
Opposite sign	127340	6240
Luminosity	7.23 pb^{-1}	0.075 pb^{-1}
Exclusive efficiency	0.159	0.784
Effective (no-PU) luminosity	1.16 pb^{-1}	0.0590 pb^{-1}

TABLE I. Numbers of 2-track events after sequential requirements.

A. Raw data mass distributions

We first show numbers of events and some features uncorrected for acceptance at 1960 GeV, and then we will describe the acceptance as a function of $M(\pi\pi)$ and $P_t(\pi\pi)$ and calculate cross sections. The data selection is $|\eta(\pi)| < 1.3$, $P_t(\pi) > 0.4\text{GeV}/c$, and $|y(\pi\pi)| < 1.0$, and no other particles in $|\eta| < 5.9$. Even before correcting for acceptance we note several qualitative features of the data.

Fig. 1 and Fig. 2 shows the mass distributions of the events in $10 \text{ MeV}/c^2$ bins, for all P_t , with statistical errors only, assuming that h^+h^- is $\pi^+\pi^-$. Above $5 \text{ GeV}/c^2$ there are only a few events. At both energies there is a large asymmetric peak between $1.0 < M(\pi\pi) < 1.5$

CDF Run II Preliminary

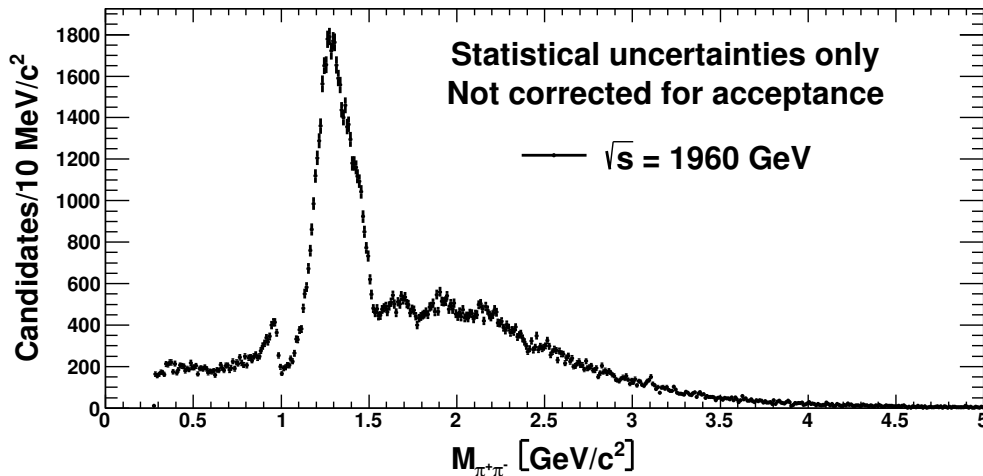


FIG. 1. Invariant mass distribution of two particles assuming pion mass - not corrected for acceptance at $\sqrt{s} = 1960$ GeV.

GeV/c², in the region of the $f_2(1270)$ and $f_0(1370)$ mesons. Later we present a partial wave analysis (PWA) of the data. Other features visible in Fig. 1, thanks to its high statistics, are (a) a very small peak at about 380 MeV/c², attributed to photoproduced $\phi \rightarrow K^+K^-$ with the kaons incorrectly assigned the pion mass (b) a peak just below 1 GeV/c², attributed to the $f_0(980)$ (c) an abrupt change of slope (almost a dip) at 1.5 GeV/c² (d) possible “ripples” between 1.5 and 2.5 GeV/c² (the acceptance in this region must at least be smooth) (e) at 3.1 GeV/c² there is a small peak attributed (in Section 11) to photoproduction of the $J/\psi \rightarrow \ell^+\ell^-$ (we did not accept events with muon stubs, but muons from low- P_t J/ψ can range out in the calorimeters, and $J/\psi \rightarrow e^+e^-$ decays will be included).

II. ACCEPTANCE CALCULATION

All cross sections presented are required to be in a certain kinematic region, namely $P_t(\text{track}) > 0.4$ GeV/c, $|\eta(\text{track})| < 1.3$, $|y(X)| < 1.0$. The P_t and η requirements allow to accept only well-reconstructed tracks. The η and y cuts define the rapidity gap extent.

As the trigger required two towers with $E_T > 0.5$ GeV, a state with $M(X) \lesssim 1$ GeV will not be accepted if it has very small P_t . So the trigger acceptance is a strong function of both $P_t(X)$ and $M(X)$ when these are both small. We also want to avoid low- P_t tracks that are not well reconstructed. For these reasons we require both tracks to have $P_t > 400$ MeV/c.

CDF Run II Preliminary

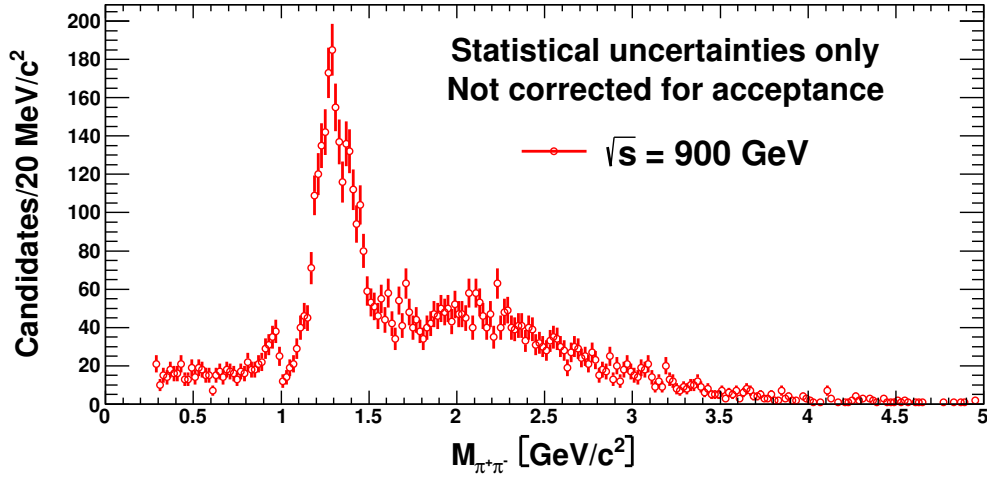


FIG. 2. Invariant mass distribution of two particles assuming pion mass - not corrected for acceptance at $\sqrt{s} = 900$ GeV.

In order to present cross sections, such as $d\sigma/(dM dP_t)$ in $|y| < 1.0$ we determine the acceptance $A(P_t(\pi^+), P_t(\pi^-), \eta(\pi^+), \eta(\pi^-), M_{\pi^+\pi^-}, P_t(X), y(X))$ using generated samples of MC events. The acceptance as a function of $P_t(\pi^+), P_t(\pi^-), \eta(\pi^+)$ and $\eta(\pi^-)$ is calculated using single pion simulation. After reconstruction using CDFSIM the event is checked if the track was reconstructed, and then, if it passed all track quality cuts. The single track acceptance was fitted with the smooth empirical estimate:

$$a \left(\frac{1}{1 + \exp(b_1 P_t + b_2)} + b_3 \right) \left(\frac{1}{(1 + \exp(c_1 \eta + c_2))(1 + \exp(-c_1 \eta + c_2))} + c_3 \right), \quad (1)$$

where a, b_i and c_i are free parameters. The result is presented in Fig. 3.

The acceptance is dependent not only on single track properties, but on correlations between two tracks. To estimate this contribution, a parent state X is generated, flat in rapidity with $-1.0 < y < +1.0$, in mass and P_t bins from $2m(\pi)$ to 5.0 GeV/c^2 , and 0 to 2.5 GeV/c respectively. X is made to decay isotropically (S-wave, $J=0$) and the quality requirements on each reconstructed track are made. Using that sample, the cuts on 3D opening angle, difference in z between tracks and spatial separation are applied. The number of events that passes such cuts divided by sample size gives the acceptance as a function of $M(X)$ and $P_t(X)$. The results are presented in the Fig. 4.

The trigger efficiency was determined by a data-driven procedure using well measured

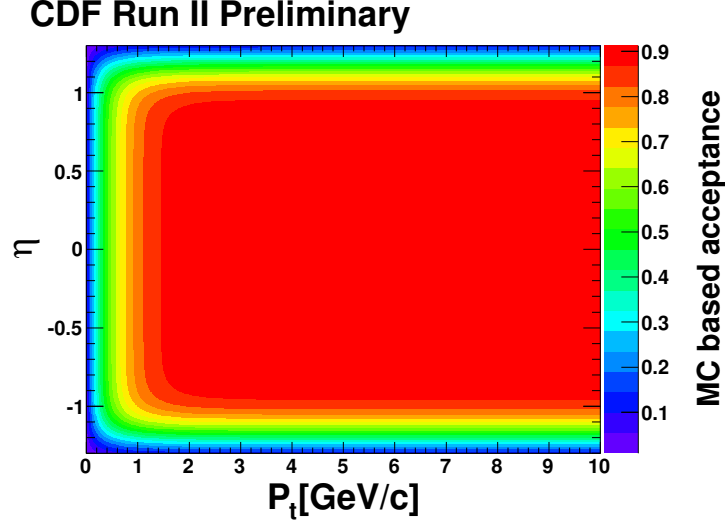


FIG. 3. Probability of a track to be reconstructed and to pass quality cuts.

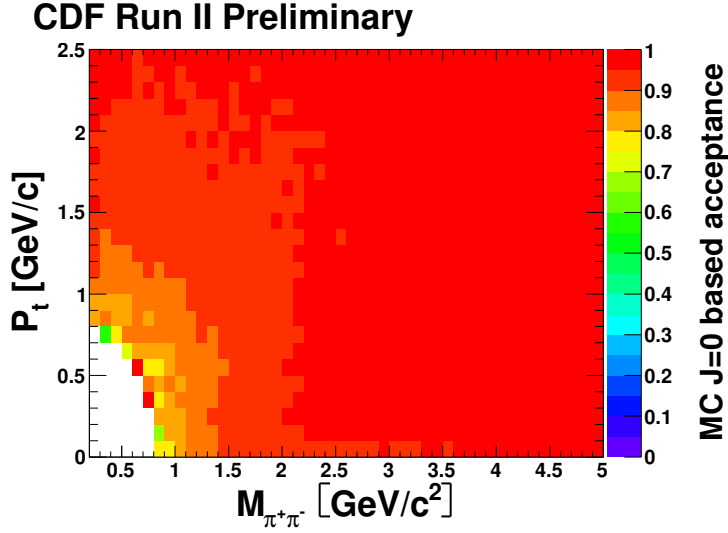


FIG. 4. Two track acceptance as a function of invariant mass and P_t after requiring both tracks to be well reconstructed.

isolated tracks from minimum-bias data from same periods. We calculated the probability of track to fire 0, 1, 2 or more trigger towers with ≥ 4 bits (0.5 GeV) in the 3x3 tower region around the extrapolated tower. The total trigger efficiency is composed of those three probabilities and computed as a function of track P_t and η values. The probabilities as a function of track P_t and η is shown in the Fig. 5.

Finally, in order not to have fake structures from statistical fluctuations in the (finite!)

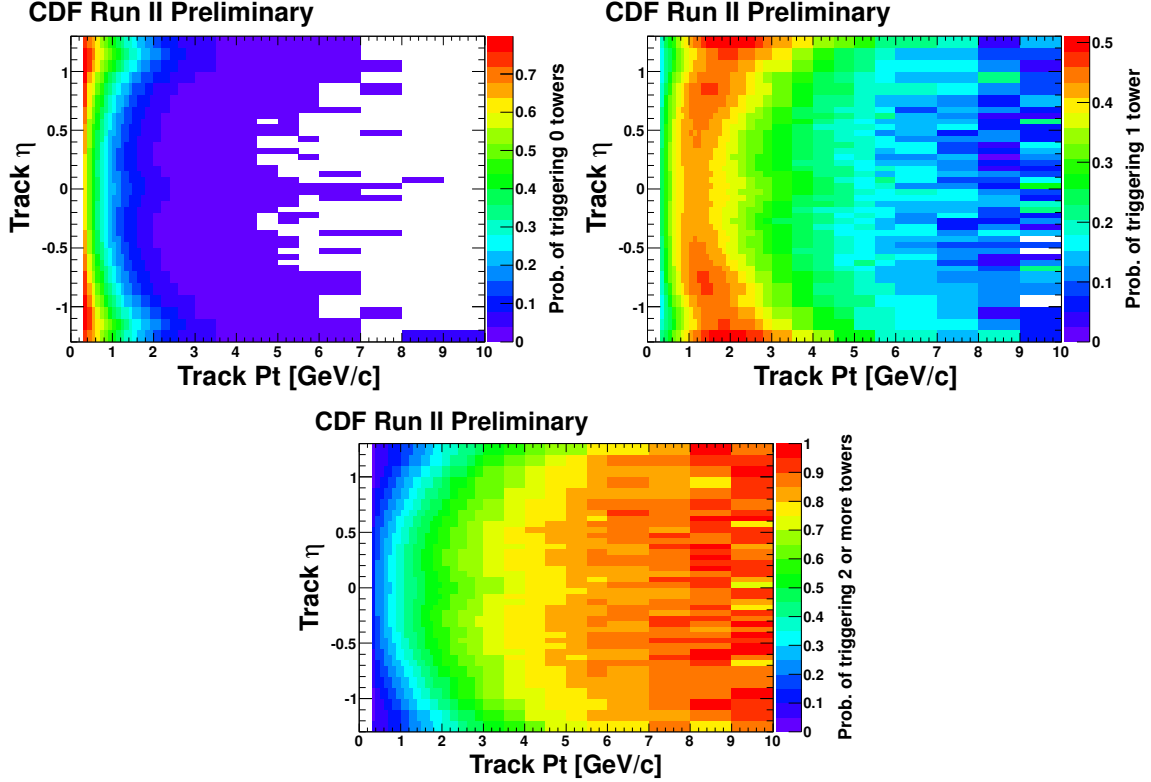


FIG. 5. The probability of triggering zero, one and two or more trigger towers as a function of track P_t and η .

Monte Carlo, we used a bilinear interpolation to compute the acceptance at every point.

III. SYSTEMATIC UNCERTAINTIES

To estimate the systematic errors we use the method of loose/tight cuts. We vary a cut by a variation of $\pm 1\sigma$ in the case of Gaussian-like distributions (e.g. P_t), or $0.5 \cdot \text{FWHM}$ in case of Lorentz-like distributions (e.g. d_0) or by a reasonable value in case of different cuts (e.g. forward cuts). The resulting shifts in the M, P_t plane are used as systematic uncertainties. Most of the errors are mass-independent. The dominant sources of systematic errors are:

- Exclusivity cuts in central region $\approx 15\%$
- Luminosity uncertainty = 6% (for $\sqrt{s} = 1960$ GeV) 10% (for $\sqrt{s} = 900$ GeV data)

The errors are assumed to be uncorrelated. Table II lists the main systematic uncertainties in the 1960 GeV cross sections. The systematic uncertainties at 900 GeV were separately evaluated and are similar, but the luminosity uncertainty is 10%.

Cut	syst. uncertainty in %	syst. uncertainty in %
	for $M_{\pi^+\pi^-} < 1.5 \text{ GeV}/c^2$	for $M_{\pi^+\pi^-} > 1.5 \text{ GeV}/c^2$
BSC gap cut	2	2
CLC gap cut	0.1	0.1
Fwd Plug gap cut	4	2
$\eta(\pi)$	0.2	0.2
$y(X)$	0.1	0.1
3D opening angle	0.1	0.1
d_0	1	1
$P_t(\pi)$	8	2
exclusivity cut	12	9
Δz_0	2	2
COT hits	4	4
χ^2/DoF of track fit	3	3
trigger efficiency	0.4	0.6
stat. error of acceptance	2	4
luminosity	6	6

TABLE II. Systematic uncertainties in cross sections distribution for $\sqrt{s} = 1960 \text{ GeV}$ data for low and high invariant mass regions.

In all plots presented in this note, systematic uncertainties are presented as yellow boxes. They were calculated for each distribution bin-by-bin, taking into consideration asymmetries of the uncertainties. Systematic errors in the mean P_t spectrum presented in Section IV C are equal to about 1%. They are mostly independent of mass. Systematic uncertainties in the Legendre coefficients spectra, presented in Section VII, are also small and mass-independent. Both of them were calculated using the same method as for the cross sections. All the applied cuts were varied and their influence on the final spectra was checked.

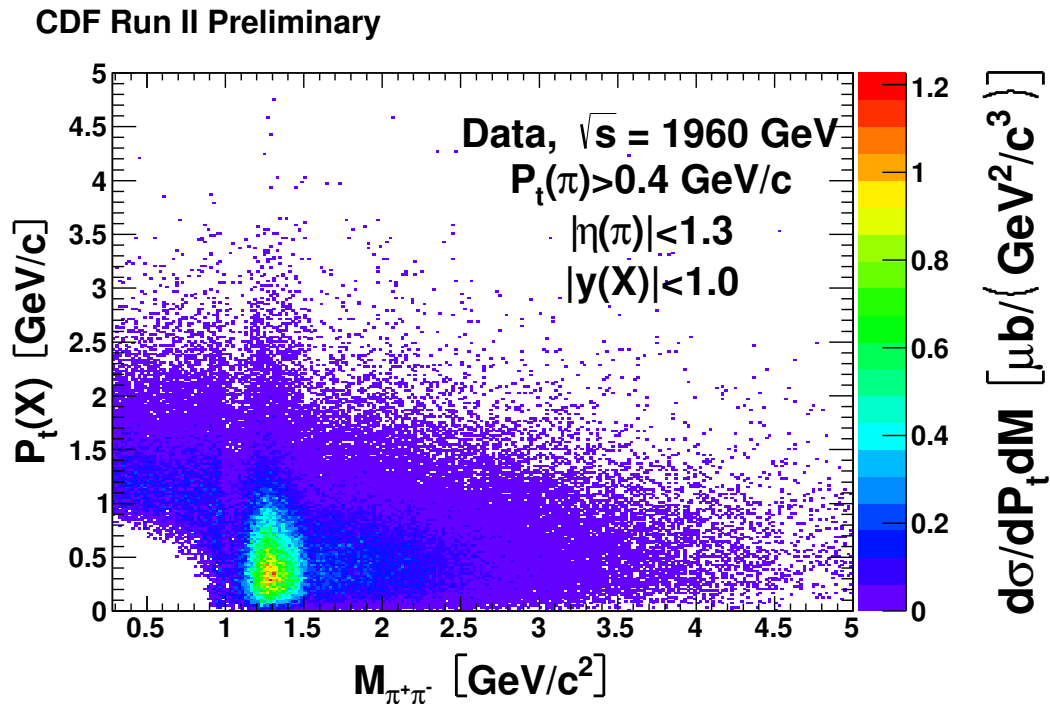


FIG. 6. Distribution of events in mass versus P_t for the $\pi^+\pi^-$ central state after acceptance corrections.

IV. $\pi^+\pi^-$ CROSS SECTIONS

For each M, P_t bin, see Fig. 6, we divide the data by the acceptance to get the corrected mass distribution, and use the effective luminosity to get the cross section $d\sigma/dM$. The invariant mass plot integrated over the full P_t range for 1960 GeV is shown in Fig. 7. The comparison of two energies (1960 GeV and 900 GeV) is shown in Fig. 8. Fig. 9 presents ratio of invariant mass distributions for two different \sqrt{s} . Additionally, to skip the region close to the $P_t(X)$ vs $M(\pi\pi)$ area where two tracks acceptance equals zero (because of kinematic cut $P_t(\pi) \geq 0.4 \text{ GeV}/c$) we are presenting invariant mass distributions for $P_t(X) > 1 \text{ GeV}/c$ and whole mass range for both \sqrt{s} (see Fig. 10 and 11). We now discuss the different features of the fully-corrected cross section. (It still contains some non- $\pi\pi$ background, shown later to be small.)

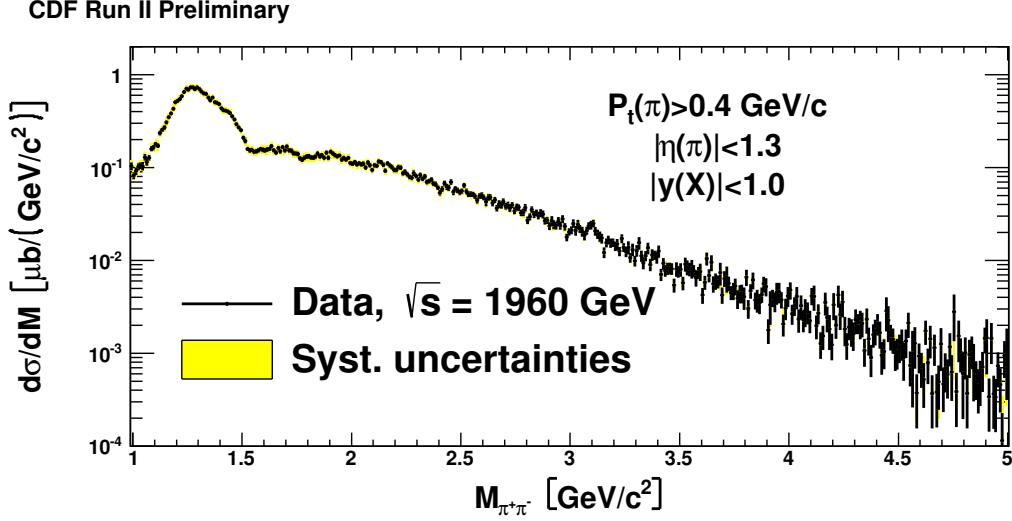


FIG. 7. Invariant mass distribution of two particles assuming pion masses - corrected for acceptance, on a logarithmic scale, $\sqrt{s} = 1960 \text{ GeV}$.

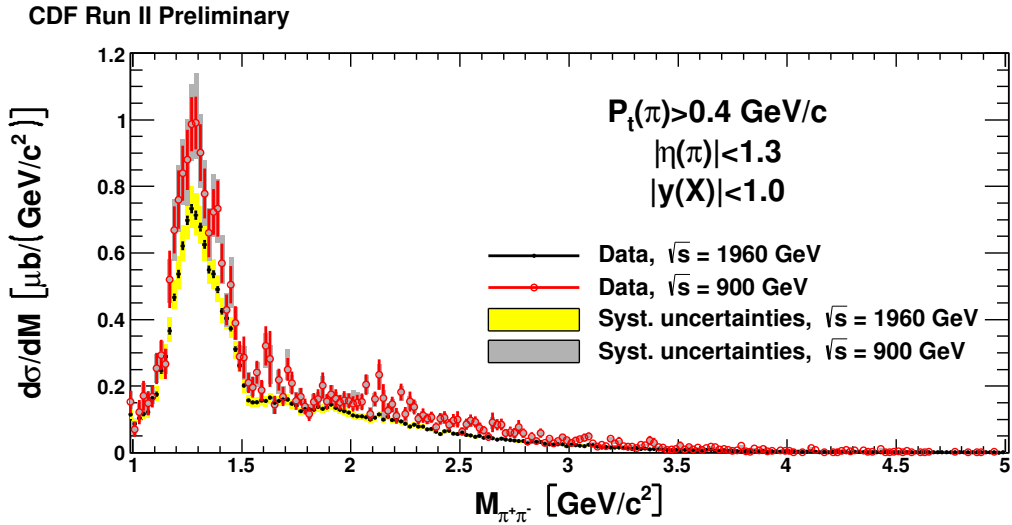


FIG. 8. Comparison of invariant mass distribution of two particles assuming pion masses - corrected for acceptance, for two \sqrt{s} energies, 1960 GeV - black and 900 GeV - red.

A. Region 0.8-2.0 GeV/c^2

This region consists of the most clearly visible resonances and a continuum $\pi^+\pi^-$ distribution. One can not simply add resonance signals and “background”, as they are both results of interference and scattering between the final state pions. We can clearly see a sharp drop at the opening of K^+K^- threshold, then the large peak coming from (proba-

CDF Run II Preliminary

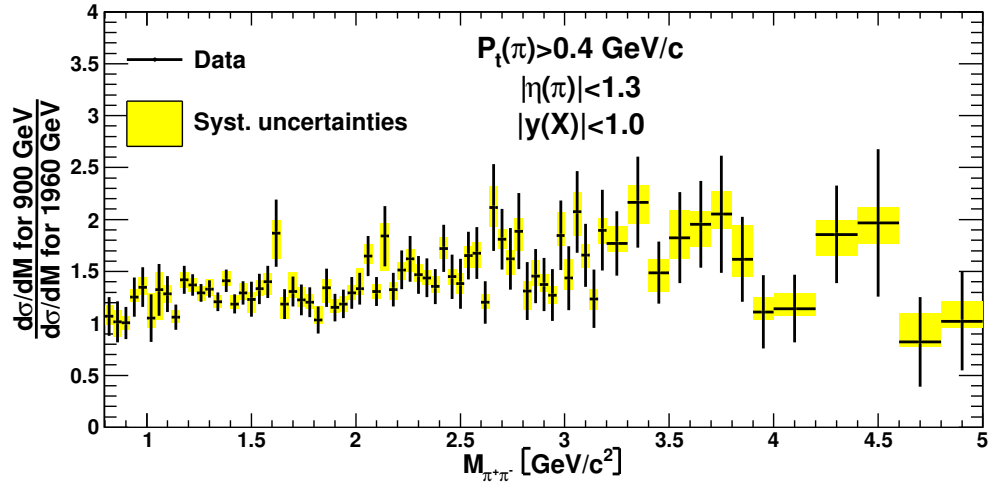


FIG. 9. Ratio of cross sections measured at 900 GeV and 1960 GeV.

CDF Run II Preliminary

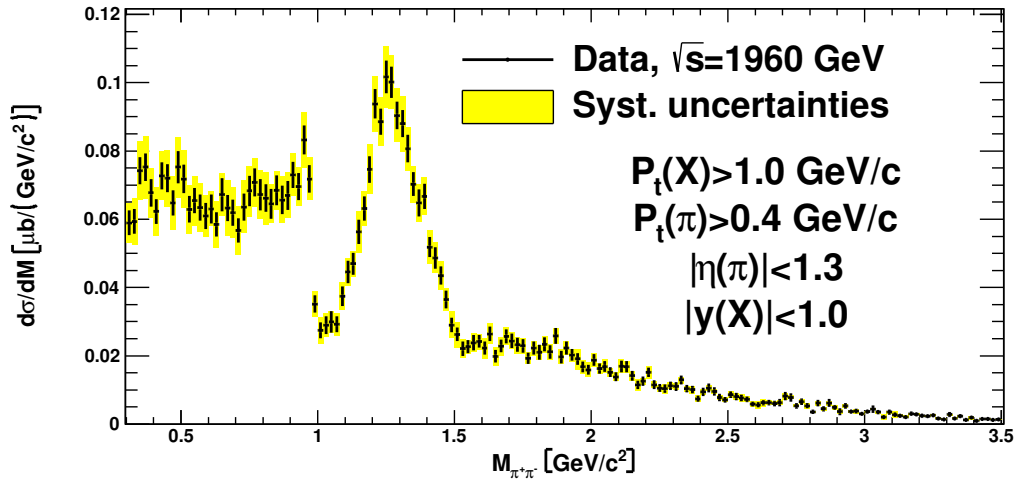


FIG. 10. Invariant mass distribution of two particles assuming pion masses for $P_t(X) > 1$ GeV/ c for $\sqrt{s} = 1960$ GeV.

bly) the $f_2(1270)$ state, although our partial wave analysis (Section 12) shows the decay to be isotropic. This peak shows structure that is not well approximated by single resonance (Breit-Wigner or Gaussian) and may be due to the $f_0(1370)$. Above this large peak, at 1.5 - 1.6 GeV/ c^2 , we see a clear and localized change of slope. All these features are clearly visible in Fig. 10 and 12.

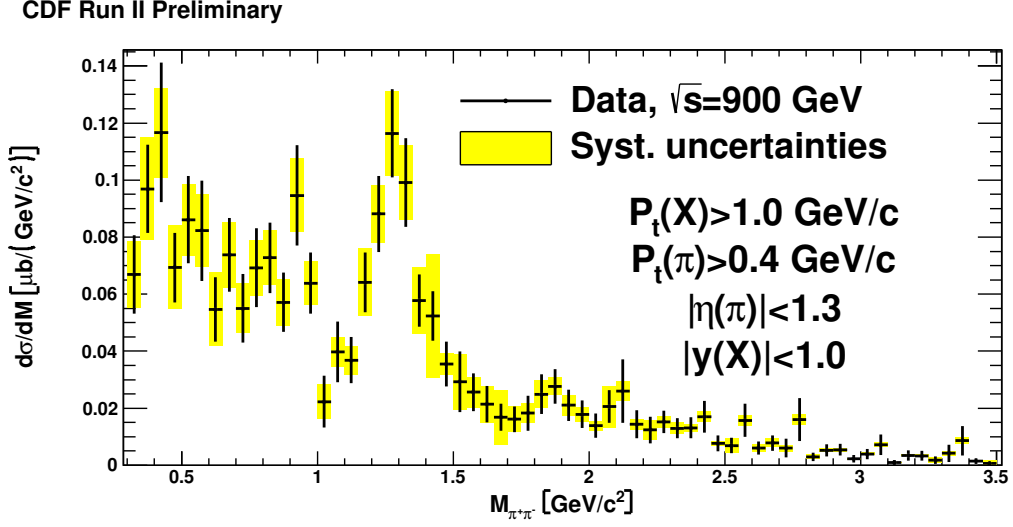


FIG. 11. Invariant mass distribution of two particles assuming pion masses for $P_t(X) > 1 \text{ GeV}/c$ for $\sqrt{s} = 900 \text{ GeV}$.

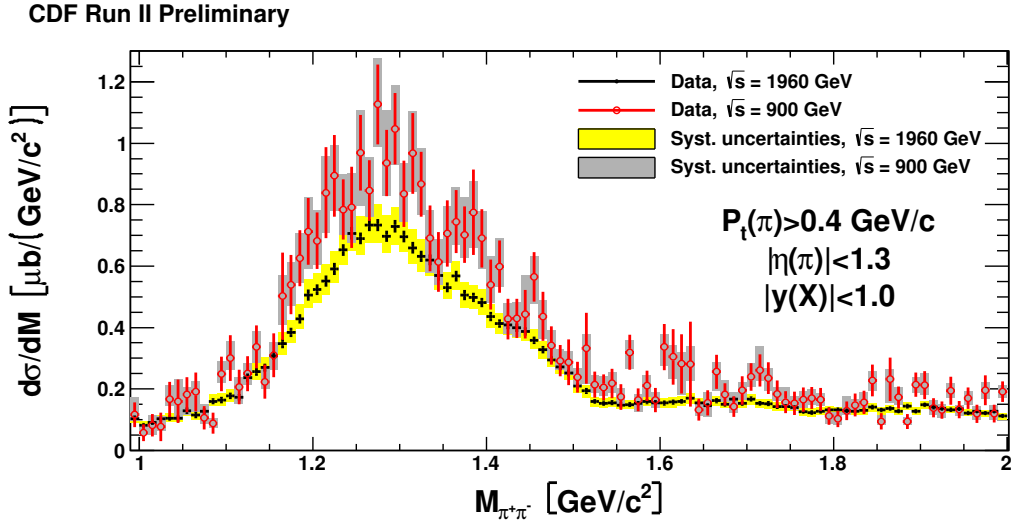


FIG. 12. Comparison of invariant mass distribution of 2 particles assuming pion masses - corrected for acceptance, for two \sqrt{s} energies, 1960 GeV - black and 900 GeV - red.

B. Region $1.6 - 5.0 \text{ GeV}/c^2$

The region above the most prominent resonances shows a bump structure, not very consistent with simple curve. Some broad f_0/f_2 states might be present there, interfering with a continuum background. Our statistics are not high enough to resolve any such

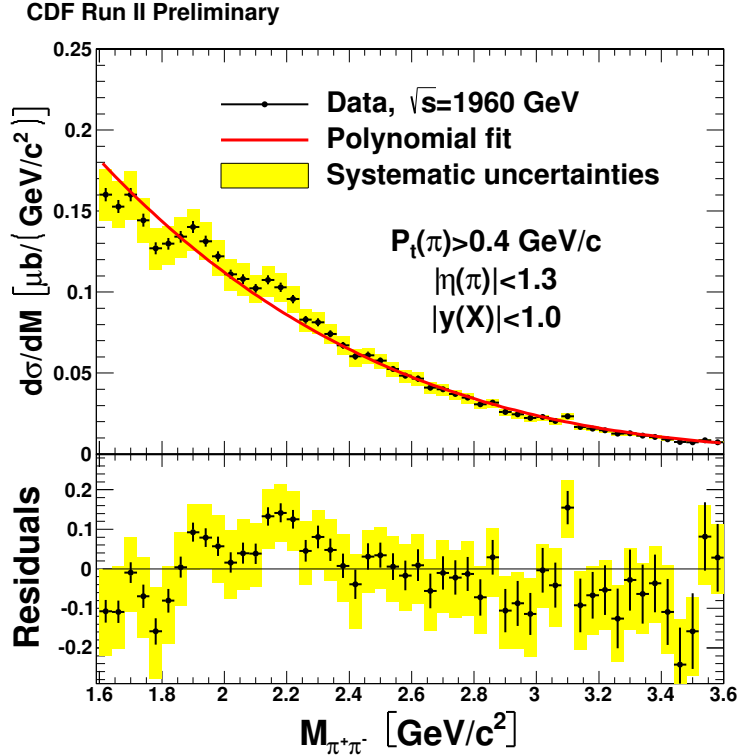


FIG. 13. Invariant mass distribution of 2 particles assuming pion masses - corrected for acceptance with 4th order polynomial fit together with residuals of the fit, $\sqrt{s} = 1960$ GeV.

states, but are enough to show the discrepancies from smooth fits. We tried to fit a 4th order polynomial, see Fig. 13, fit to this region, which shows also the residuals. Statistically (black bars) the structures are significant, and the systematic uncertainties (yellow band) are not bin-dependent. The high point at about $3.1 \text{ GeV}/c^2$ is the J/ψ (Section 11).

C. Mean P_t

Another interesting kinematic variable is the P_t of central state. In Figs. 14 and 15 show the dependence of $\langle P_t \rangle$, corrected for acceptance, on the invariant mass. This distribution shows interesting structure not significantly dependent of the \sqrt{s} energy. It has been already shown that the acceptance has a cut-off at low P_t for $M(\pi\pi) < 0.8 \text{ GeV}/c^2$, so we only show this for $M(\pi\pi) > 1 \text{ GeV}/c^2$ where the acceptance distortion is not too strong. The main feature of this plot is the rather localized increase in $\langle P_t \rangle$ at $1.5 \text{ GeV}/c^2$, coinciding with the change in slope of the mass spectrum, and not due to any rapid change of the acceptance. There may also be some features above $2 \text{ GeV}/c^2$. A few of the distributions of P_t (for some

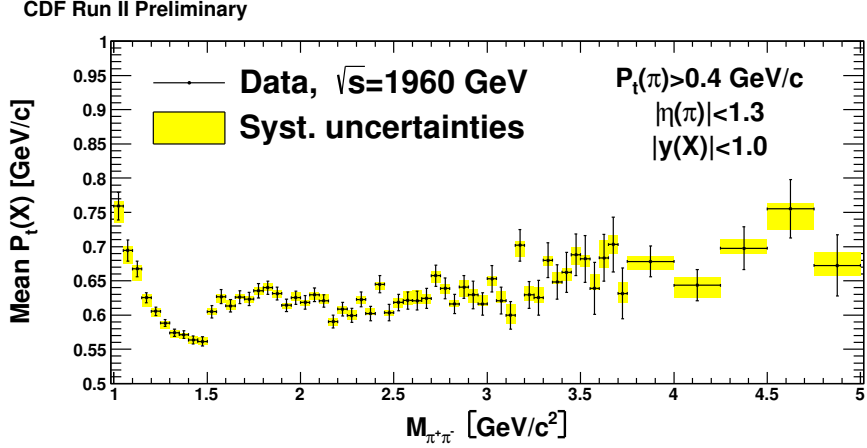


FIG. 14. Mean value of the P_t distribution of the central state decaying to two central pions as a function of invariant mass, $\sqrt{s} = 1960$ GeV.

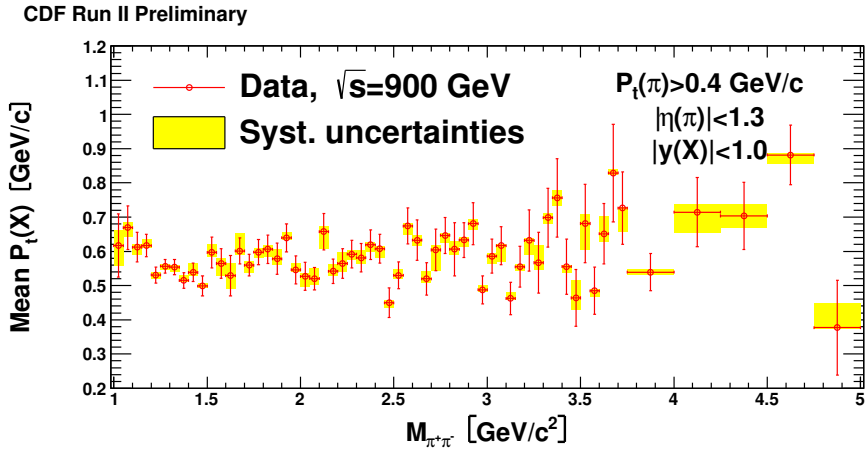


FIG. 15. Mean value of the P_t distribution of central state decaying to two central pions as a function of invariant mass, $\sqrt{s} = 900$ GeV

mass ranges) are shown in Fig. 16.

V. EXCLUSIVE χ_{c0} PRODUCTION IN $\chi_{c0} \rightarrow \pi^+\pi^-$ AND K^+K^- .

We previously observed [3] exclusive DIPE production of $\chi_c(c\bar{c}) \rightarrow J/\psi + \gamma \rightarrow \mu^+\mu^-\gamma$ with a cross section $d\sigma/dy|_{y=0} = 76 \pm 10(\text{stat}) \pm 10(\text{syst})$ nb (7.6×10^{-32} cm²), assuming all the events were $\chi_{c0}(3415)$. This corresponded to 65 candidate events. The process is especially important because the χ_{c0} has the same quantum numbers as the Higgs boson (apart from

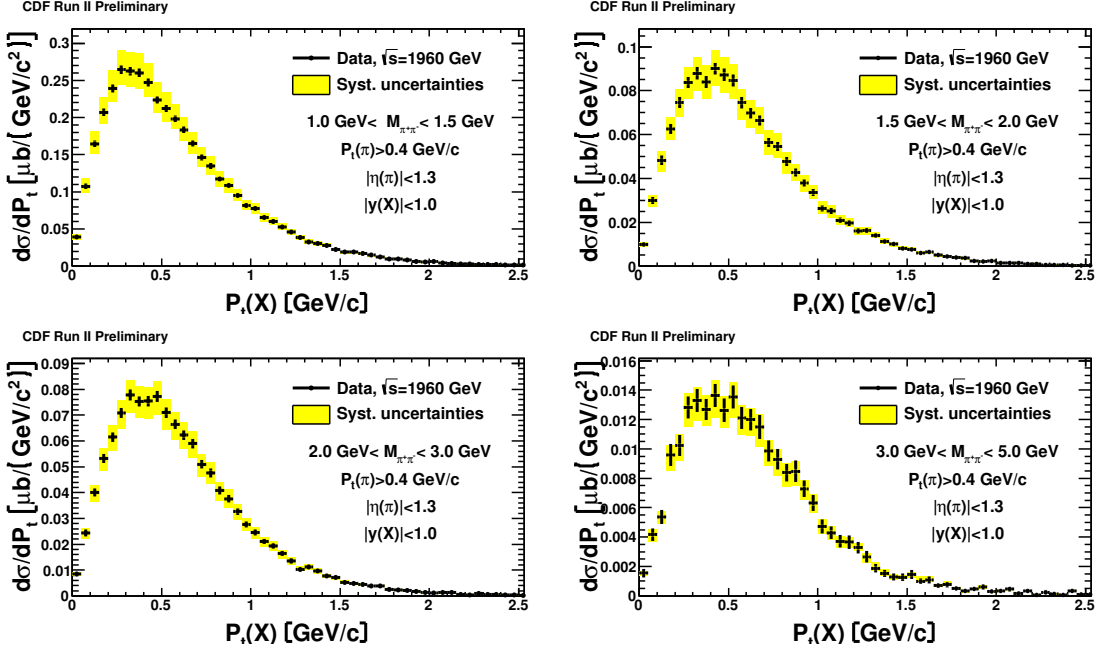


FIG. 16. P_t distribution of central state decaying to two central pions in few mass windows, $\sqrt{s} = 1960$ GeV.

its strong interactions) and is produced the same way but with a c -loop replacing the t -loop, so it is a good control of the theoretical calculations. Unfortunately in the exclusive $\chi_c \rightarrow J/\psi + \gamma$ channel the photon is soft and the mass resolution of $J/\psi + \gamma$, together with the poor energy resolution of the EM calorimeter, did not allow a separation of the three χ_c^0 states. The $J=1$ and $J=2$ states should theoretically be suppressed in production (in D IPE) but they have larger branching fractions to this mode, see Table IV, which also shows the decays to only charged hadrons that have branching fractions $\gtrsim 0.1\%$ for the χ_{c0} .

As we could not resolve the three χ_c states we actually measured $\sum_{i=0,2} B_{ci} \cdot \sigma_{ci}$ where the branching fractions to $J/\psi + \gamma$ from the PDG [5] are given in Table IV. Even though the $\chi_{c1}(3511)$ and $\chi_{c2}(3556)$ are theoretically very suppressed they may contribute a lot to the $J/\psi + \gamma$ signal. Observation in the $\pi^+\pi^-$ and K^+K^- channels can resolve the states, not only because the mass resolution $\sigma(m) \sim 25$ MeV is less than their separation but also because the decay fractions are higher (than the combination $\chi_c \rightarrow J/\psi + \gamma \rightarrow \mu^+\mu^- + \gamma$). In the two cases, “all χ_{c0} ” or “a mixture of all three” (B = branching fraction):

$$B_{c0}\sigma_{c0}(\text{if - alone}) \equiv [B_{c0}\sigma_{c0} + B_{c1}\sigma_{c1} + B_{c2}\sigma_{c2}](\text{if - all - three})$$

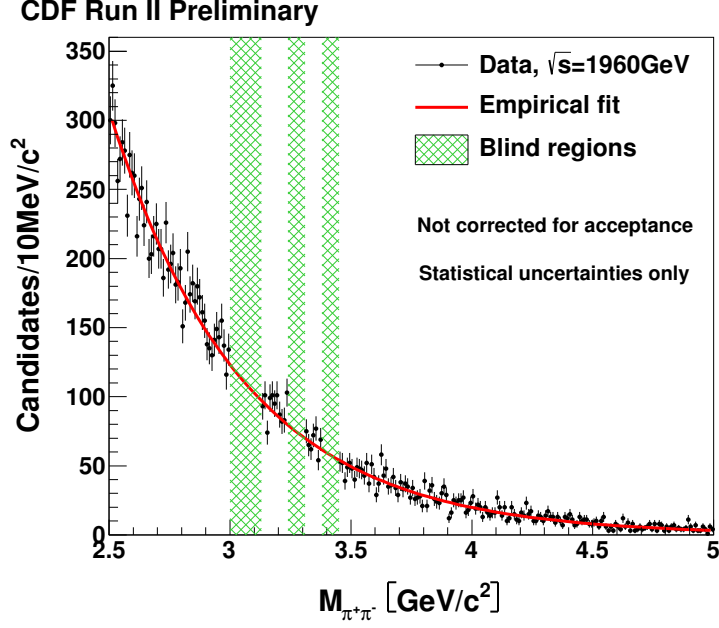


FIG. 17. Invariant mass distribution of two particles, assumed to have $m(\pi)$, in the charmonium region at $\sqrt{s} = 1960 \text{ GeV}$. The regions of the J/ψ and χ_{c0} (in both $\pi^+\pi^-$ and K^+K^- modes) are excluded from the fit.

and dividing through by B_{c0} :

$$\sigma_{c0}(\text{if - alone}) \equiv \sigma_{c0} + (B_{c1}/B_{c0} = 26.8) \times \sigma_{c1} + (B_{c2}/B_{c0} = 17.1) \times \sigma_{c2}$$

Let us take as an example the predictions of Teryaev, Pasechnik and Szczurek [6] for the relative cross sections $d\sigma/dy|_{y=0}$ of the three states. There are large uncertainties, depending on parameters, but they expect approximately $\sigma_{c0} : \sigma_{c1} : \sigma_{c2} = 1.0 : 0.006 : 0.09$. In that example we would have:

$$\sigma_{c0}(\text{true}) = \sigma_{c0}(\text{if - alone}) \times 1/(1 + 26.8 \times 0.006 + 17.1 \times 0.09) = 0.37 \times \sigma_{c0}(\text{if - alone})$$

and then $\sigma_{c0}(\text{true})$ would be $\sim 0.37 \times 76 \text{ nb} = 28 \text{ nb}$.

The new $\pi^+\pi^-$ and K^+K^- data presented here can provide a measurement (in practice an upper limit) of $d\sigma/dy|_{y=0}$. The data in Fig. 7 do not show a significant $\chi_{c0}(3415)$ signal. In Fig. 17 we show the number of events between 2.5 and 5.0 GeV/c^2 together with a fit excluding the regions of the J/ψ and $\chi_{c0} \rightarrow \pi^+\pi^-, K^+K^-$ (with the K given the pion mass). The fit is an exponential with slope -1.876 GeV^{-1} . Table III presents results. They rule out the supposition that all the $J/\psi + \gamma$ events in Ref.[3] were from χ_{c0} and would be consistent

TABLE III. Upper limits on χ_{c0} cross sections.

State:	$\chi_{c0} \rightarrow \pi^+\pi^-$	$\chi_{c0} \rightarrow K^+K^-$
Background (est.)	404.4	522.1
Events in window	424	515
90% CL upperlimit (events)	49.3	34.6
Acceptance	21.4%	21.3%
$d\sigma/dy _{y=0}$, 90% CL UL	35.5 nb	23.4 nb

with the 17% fraction seen by LHCb (although they are at a different \sqrt{s} and in a different y -region, and also not published).

VI. EVIDENCE FOR $J/\psi \rightarrow e^+e^-$

The mass distribution has a small excess in the vicinity of the $J/\psi(3097)$. Photoproduction of J/ψ with decays to $\mu^+\mu^-$ was previously observed in CDF [3], with $d\sigma/dy(y=0) = 3.92 \pm 0.62$ nb, compared with several theoretical predictions for $p + \bar{p} \rightarrow p + J/\psi + \bar{p}$ from 2.8 - 3.4 nb. The measured CDF value had been reduced by $9 \pm 2\%$ to account for unseen fragmentation, with $|\eta| > 7.4$. The present measurements allow fragmentation with products between $|\eta| = 5.9$ and $y(\text{beam}) = 7.64$ and so should be larger. The only non-rare J/ψ decays to just two tracks are to e^+e^- and $\mu^+\mu^-$, each about 5.9%. Most of the $\mu^+\mu^-$ decays should be excluded by our muon stub cut. The e^+e^- events should be in our sample. Those events, with the tracks incorrectly given the pion mass, should appear at about 3.112 MeV, only 12 MeV higher. (Any $\mu^+\mu^-$ events would be at about 3.105 MeV. These are values for a J/ψ at rest, but are approximately true for our kinematics.) To quantify the excess in this data we fitted the mass distribution over the range $2.9 < M(\pi^+\pi^-) < 3.5$ GeV/ c^2 to an exponential background, excluding 3.06 - 3.14 GeV, plus a Gaussian constrained to have a peak in that range but otherwise with centre, width and size floating. See Fig. 18. The fit gives mean value at 3.097 ± 0.003 GeV/ c^2 , width $\sigma = 12.7$ MeV/ c^2 and significance 4.46σ .

We can assume the events are mostly $J/\psi \rightarrow e^+e^-$, since most $\mu^+\mu^-$ decays will be excluded by the muon stub veto. Simply as a check that the apparent signal is reasonable in magnitude, we count the excess events in the fitted peak (76), and with an acceptance

TABLE IV. Branching fractions (BF in %) of χ_c states, for decays to all charged particles with BF $> 0.1\%$.

State $I^G J^{PC}$	$\chi_{c0}(3415)$ 0^+0^{++}	$\chi_{c1}(3511)$ 0^+1^{++}	$\chi_{c2}(3556)$ 0^+2^{++}
Mass(MeV):	3414.76 ± 0.35	3510.66 ± 0.07	3556.20 ± 0.09
Width (MeV):	10.4 ± 0.7	0.89 ± 0.05	2.06 ± 0.12
BF(Channel)			
$J/\psi + \gamma$	1.16 ± 0.08	35.6 ± 1.9	20.2 ± 1.0
Above with $J/\psi \rightarrow \mu^+\mu^-$	0.077	0.021	0.012
$\pi^+\pi^-\pi^+\pi^-$	2.27 ± 0.19	0.76 ± 0.26	1.11 ± 0.11
$\pi^+\pi^-K^+K^-$	1.80 ± 0.15	0.45 ± 0.10	0.92 ± 0.11
$3(\pi^+\pi^-)$	1.20 ± 0.18	0.58 ± 0.14	0.86 ± 0.18
$\pi^+\pi^-$	0.56 ± 0.03	<0.1	0.159 ± 0.009
K^+K^-	0.60 ± 0.03	<0.1	0.11 ± 0.008
$\pi^+\pi^-K_s^0K_s^0$	0.58 ± 0.11	<0.1	0.92 ± 0.11
Above with $K_s^0 \rightarrow \pi^+\pi^-$	0.27 ± 0.05	<0.1	0.43 ± 0.05
$K^+K^-K^+K^-$	0.28 ± 0.03	0.06 ± 0.01	0.18 ± 0.02
$\pi^+\pi^-p\bar{p}$	0.21 ± 0.07	<0.1	0.13 ± 0.03
Total %	7.2	1.9	4.7

for $J/\psi \rightarrow \ell^+\ell^-$ of 20% (compared with 24.2% for $\chi_{c0} \rightarrow \pi^+\pi^-$), using the B.R in Table IV, we find $d\sigma/dy|_{y=0}(J/\psi) = 2.67$ nb. We do not give errors, as we do not think a full error analysis is worthwhile (in contrast our observation [3] in the $\mu^+\mu^-$ -channel had practically zero background). Our paper [3] gave $d\sigma/dy|_{y=0}(J/\psi) = 3.92 \pm 0.25$ (stat) ± 0.52 (syst) nb. Clearly our new data is consistent with this, and we can conclude that the peak in Fig. 18 is indeed the J/ψ ; this verifies that our mass scale is correct to about 12 MeV, and the mass resolution is better than $\sigma = 15$ MeV.

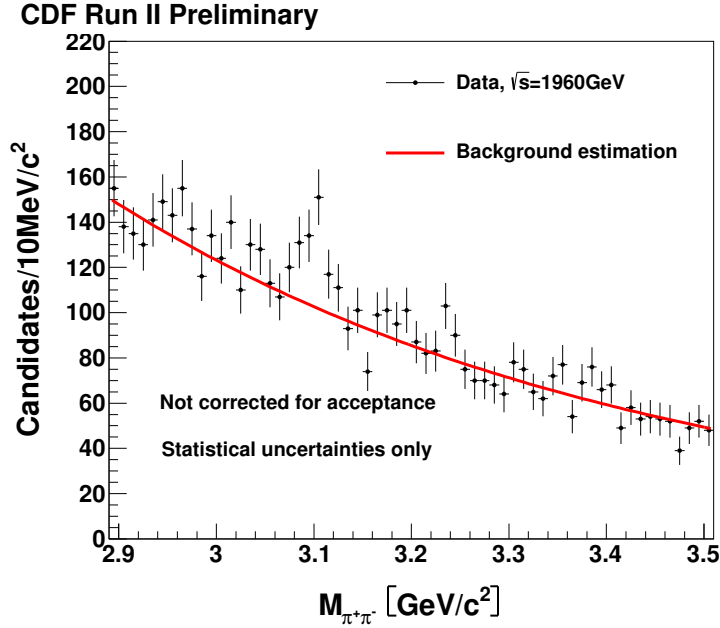


FIG. 18. Invariant mass distribution of 2 particles in the J/ψ region. with the same fit as in Fig. 17, which excludes $M(J/\psi) \pm 3\sigma$.

VII. PARTIAL WAVE ANALYSIS

In the AFS experiment [4] both protons were measured as well as the central $\pi^+\pi^-$. A partial-wave analysis (PWA) was done and showed the data to be dominated by S-wave ($J=0$) below $1.1 \text{ GeV}/c^2$, apart from a small P-wave at the ρ -mass, not visible in the mass distribution, and assumed to be ρ -photoproduction. A small D-wave signal is present between 1.2 and $1.5 \text{ GeV}/c^2$ and again at higher masses, see Fig. 11b of Ref. [4]. In this data we do not have the forward protons, which can therefore dissociate, and due to the rapidity gap requirement we have a rather limited angular acceptance. However, we can distinguish between different spin behavior by comparing data to MC sample with pre-defined spin content.

As a first step we test the “S-wave only” hypothesis, by comparing $\cos\theta$ distributions (θ - production angle) of data and Monte Carlo. To do this, we use the the Smirnow test with λ -Kolmogorov statistics, taking anything other than pure S-wave as an alternative hypothesis. The test is done in mass bins of $50 \text{ MeV}/c^2$ from 0 - $2 \text{ GeV}/c^2$, $100 \text{ MeV}/c^2$ from 2 - $4 \text{ GeV}/c^2$ and $200 \text{ MeV}/c^2$ from 4 - $5 \text{ GeV}/c^2$. The p-value of the test is shown in Fig. 19. Above $1.5 \text{ GeV}/c^2$ the pure S-wave hypothesis is excluded at 99% C.L. The $\cos\theta$ versus invariant mass

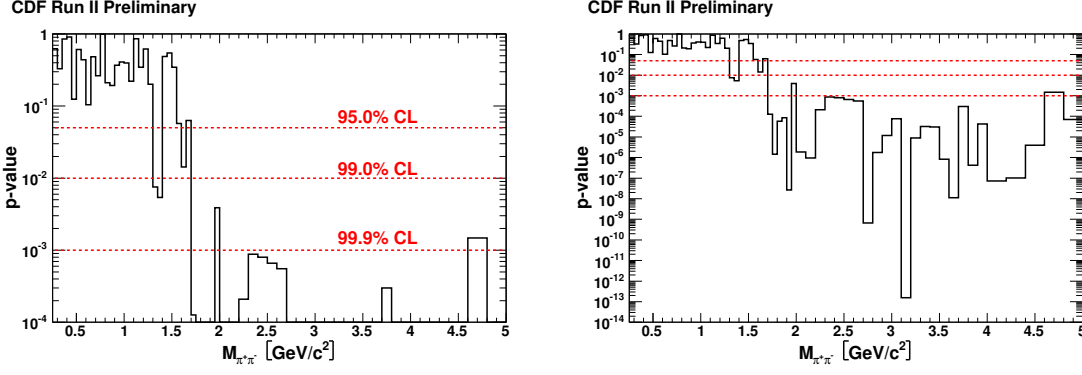


FIG. 19. (Left) p-value of Smirnov test on S-wave only hypothesis as a function of mass for $\sqrt{s} = 1960$ GeV data. We exclude the S-wave only hypothesis at 99.9% C.L. above an invariant mass of $1.51 \text{ GeV}/c^2$. (Right) The same plot on an extended scale.

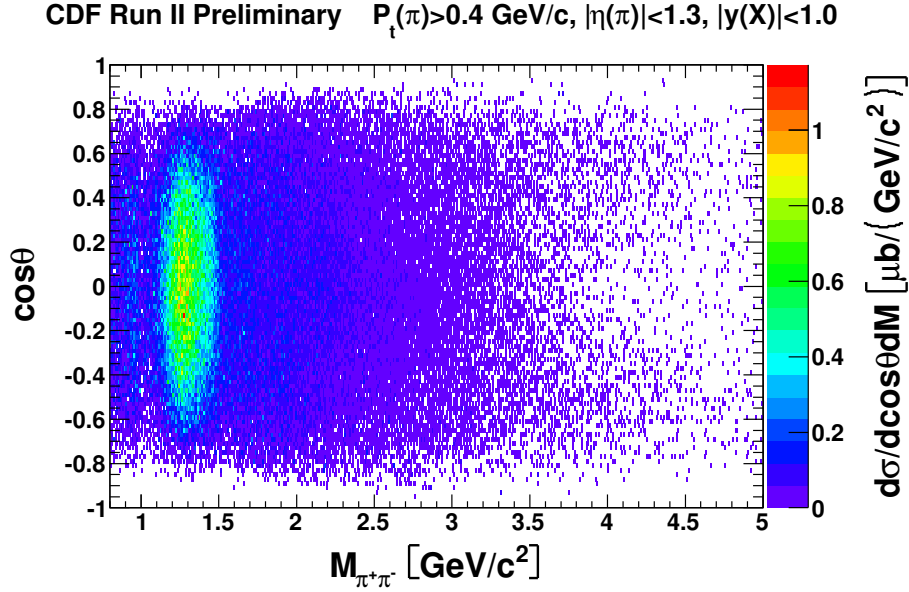


FIG. 20. The differential cross section as a function of invariant mass and $\cos \theta$ for $\sqrt{s} = 1960$ GeV.

distribution is shown in Fig. 20, and on 1-dimensional plots in several mass ranges in Fig. 21. In Fig. 22 the shape of the $\cos \theta$ distribution in the data is compared with distribution from Monte Carlo-generated samples assuming pure S-wave state content.

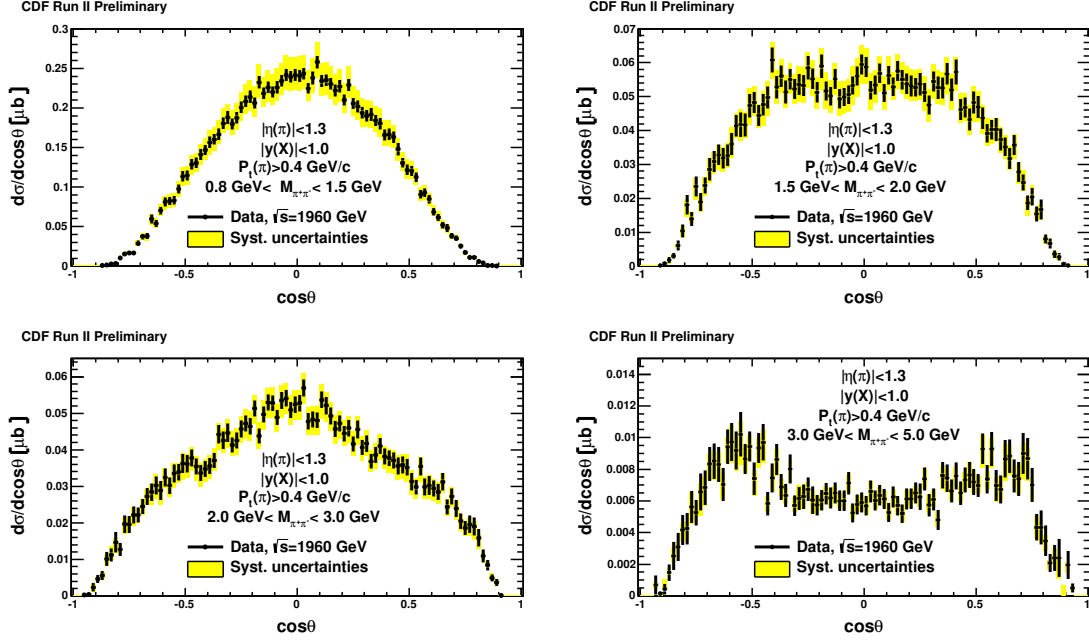


FIG. 21. Differential cross section as a function of $\cos\theta$ in several mass bins.

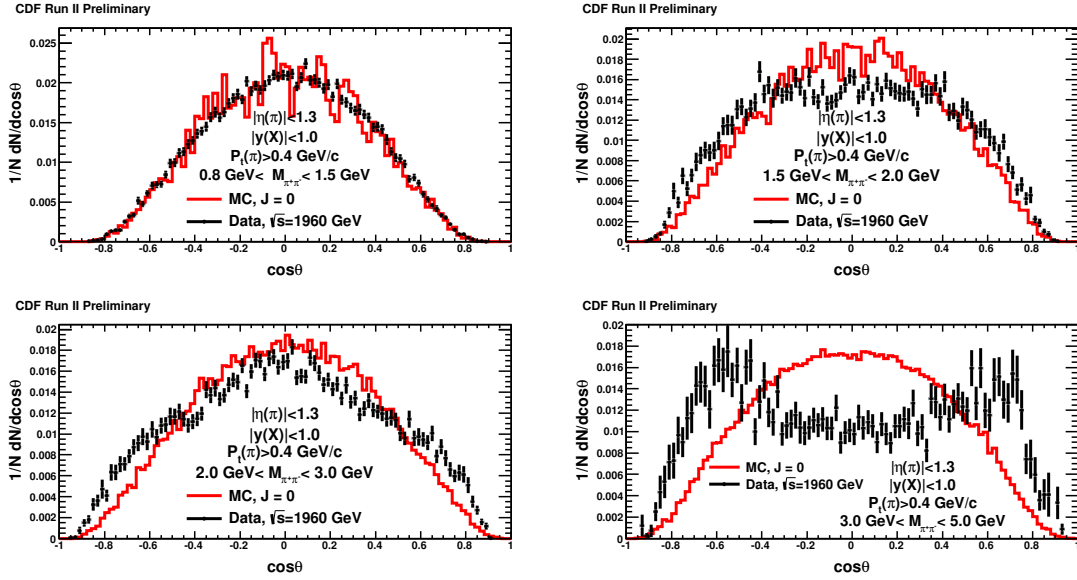


FIG. 22. Normalized $\cos\theta$ distribution in several mass bins for our data compared to MC sample with isotropic decay mode (pure S-wave).

A. Legendre polynomials

To do a more detailed analysis of spin content we decompose the $\cos\theta$ distribution in Legendre polynomials. Following the Jacob and Wick formula [7] for the $a + b \rightarrow c + d$ cross

section:

$$\begin{aligned} \frac{d\sigma}{d\Omega} &= \frac{1}{(2s_a + 1)(2s_b + 1)p^2} \sum_{(\lambda), J, J'} \left(J + \frac{1}{2}\right) \left(J' + \frac{1}{2}\right) (-1)^{\lambda - \mu} \cdot \\ &\cdot \langle \lambda_a \lambda_b | T_J(E) | \lambda_c \lambda_d \rangle^* \langle \lambda_a \lambda_b | T_{J'}(E) | \lambda_c \lambda_d \rangle \cdot \\ &\cdot \sum_{\ell} C(JJ'\ell; \lambda, -\lambda) C(JJ'\ell; \mu, -\mu) P_{\ell}(\cos \theta), \end{aligned}$$

we estimate the coefficients in front of each Legendre polynomial by calculating the weighted average:

$$a_{\ell} = \frac{\sum_i w_i P_{\ell}(\cos \theta_i)}{\sum_i w_i}, \quad (2)$$

where the sum is done over all events and w_i are weights obtained from the acceptance. We did the same analysis using MC events generated with S-wave only. In that situation one expects, having full kinematic coverage, all coefficients except the 0th to be zero (i.e. the $\cos \theta$ distribution is flat). Unfortunately, our kinematic cuts on track P_t and η strongly influence the shape of the $\cos \theta$ distribution. Results of this coefficient estimation are presented in Fig. 23.

We conclude that up to $M(\pi^+\pi^-) = 1.5 \text{ GeV}/c^2$ the data are consistent with being only (or at least, dominated by) S-wave, while above that higher waves must be introduced. We do not see a local dip in the p-value that could be caused by a dominant $f_2(1270)$ meson.

VIII. K^+K^- BACKGROUND IN $\pi^+\pi^-$ DATA.

A. Charged track identification

Thus far we have been assuming that the two charged hadrons are $\pi^+\pi^-$, without using any hadron identification. There are three main ways of estimating the K^+K^- background in each mass bin. One is to use the ionization of the COT tracks, i.e. dE/dx , which depends on the particle speed and hence its mass (for a given momentum). However it is only useful for clean π/K separation for tracks with momenta $\lesssim 400 \text{ MeV}/c$, which is our lower cut. (Protons are better separated from π/K . The $p\bar{p}$ background is negligible.)

Secondly one can use the flight time from the collision time to the Time of Flight (TOF) counters. For these exclusive h^+h^- events, the actual event time t_0 is not known better than about 1 ns, but differences in flight path length and momenta between the two particles can still often distinguish $\pi^+\pi^-$, K^+K^- , and $p\bar{p}$ events. Only 37% of the events have TOF

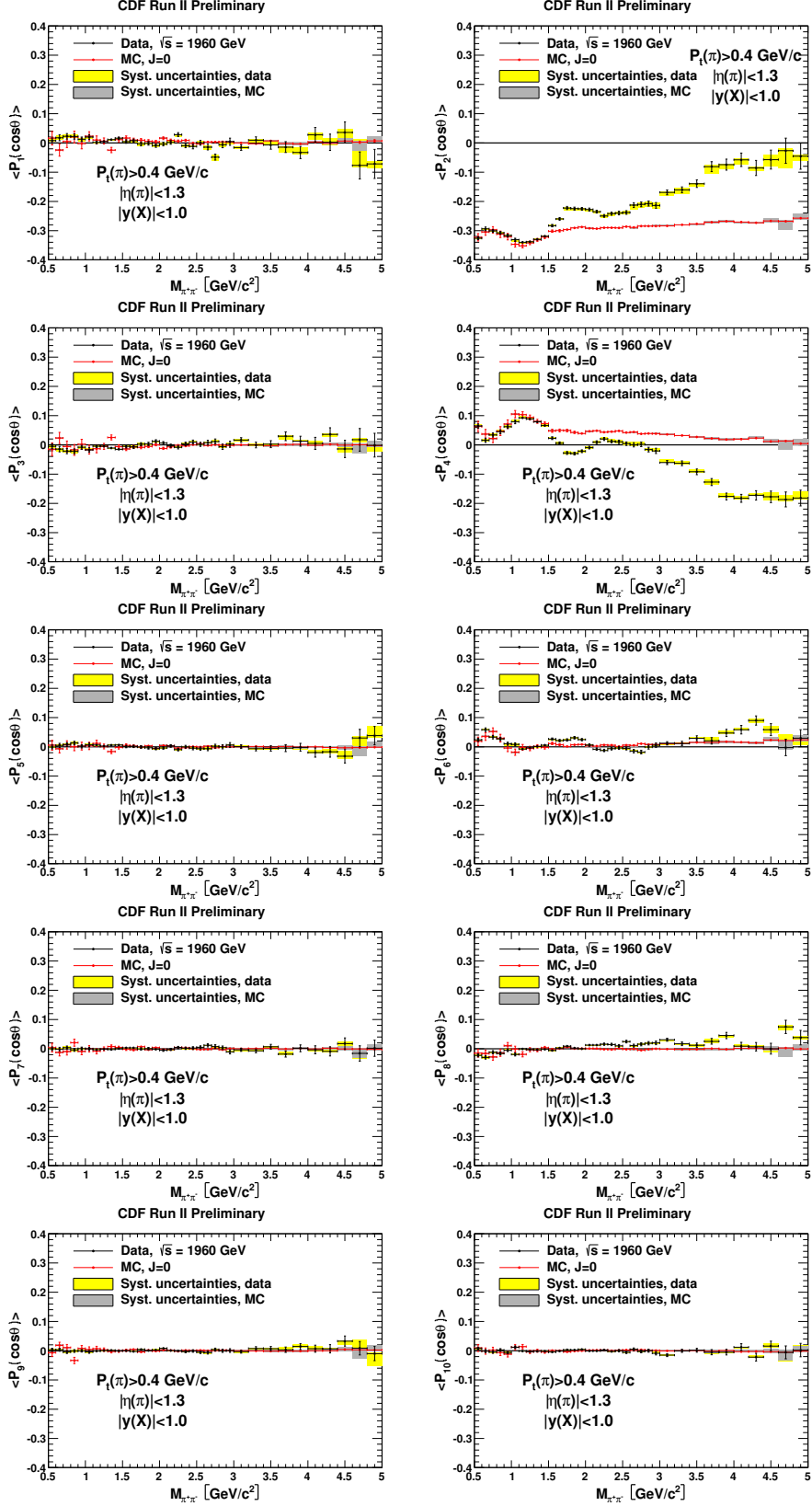


FIG. 23. First ten Legendre coefficients as a function of mass for selected sample of two tracks events for $\sqrt{s} = 1960$ GeV data and for MC sample (isotropic decay model) of two tracks events.

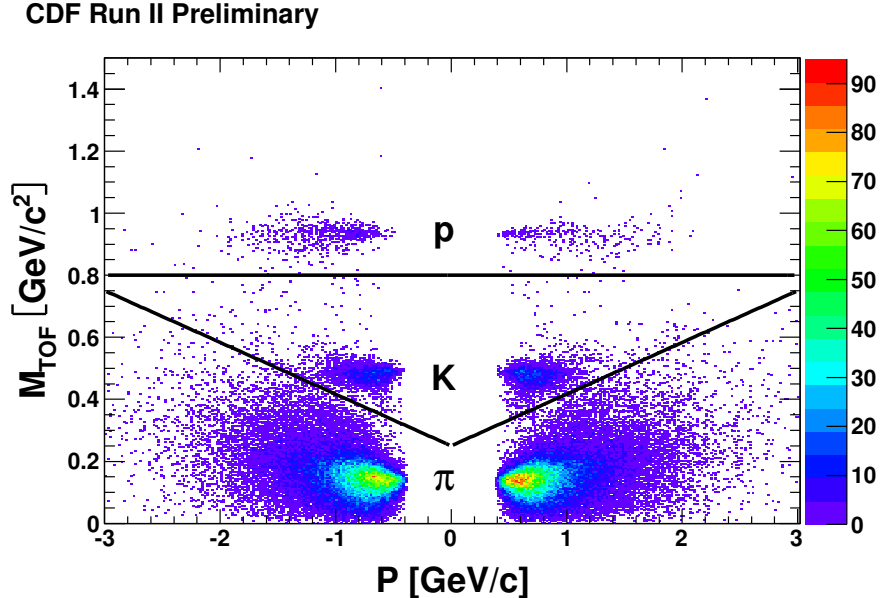


FIG. 24. Mass calculated using Time of Flight as a function of particle momentum. Visible bands correspond to pions, kaons and protons respectively. Negative momenta correspond to negatively charged particles.

information for both tracks, mainly because the TOF bars only extend to $|\eta| = 1.0$, and because the TOF bars are less efficient near the ends (signals at both ends are required).

In Fig. 24 mass calculated using TOF (M_{TOF}) versus particle momentum is shown. The negative momenta correspond to particles with negative charge. To separate $\pi/K/p$ sharp cuts presented as black lines in Fig. 24 were used. The momentum-dependent cut is empirical, to avoid the dominant pions feeding into the kaon band at high momentum, where the mass resolution is poor. Fig. 25 presents the obtained mass distribution assuming mass of two pions π with contributions coming from KK , πK , and Kp , πp , $p\bar{p}$ pairs.

A third method of estimating the K^+K^- background is to measure the $K^0\bar{K}^0$ spectrum. We selected events with four tracks consistent with two $K_S^0 \rightarrow \pi^+\pi^-$ decays (displaced vertices, K^0 mass and directionality cuts). The $K^0\bar{K}^0$ cross section should be a factor $\times 2$ higher because of unseen $K_L^0K_L^0$ events ($K_S^0K_L^0$ events are forbidden by the CP-even rule), and correcting for the branching fraction for $\pi^+\pi^-$ decays, we then have an estimate of $\sigma(K^+K^-)$. The corrections for acceptance are not yet final, so we do not yet show the background under the (assumed) $\pi^+\pi^-$ spectrum obtained by giving the kaons pion masses. However we can already conclude from the few $K_S^0K_S^0$ events that K^+K^- is a very

CDF Run II Preliminary

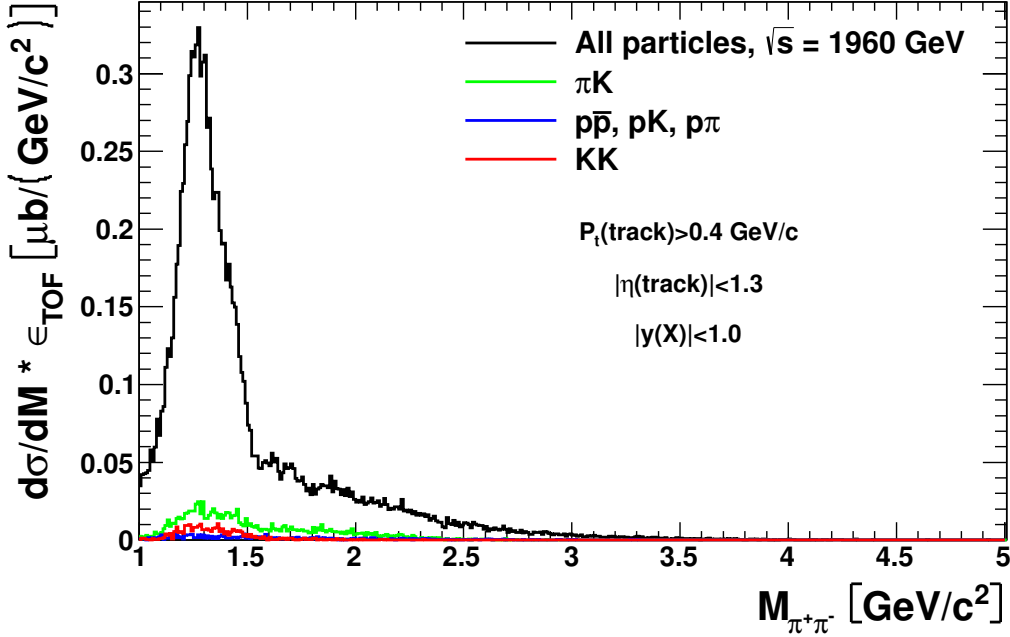


FIG. 25. Invariant mass distribution for all selected particles assuming pions masses with contributions coming from non- $\pi\pi$ background identified with TOF method.

small background in the $\pi^+\pi^-$ spectra, corroborating the estimate from K^+K^- that the background under the $\pi^+\pi^-$ cross section in this region, while mass-dependent, is everywhere $< 4\%$.

IX. ESTIMATION OF NON-EXCLUSIVE BACKGROUND

Table I shows the numbers of events at several stages of the analysis. One can see that the events with two same charge tracks are 6.1% and 7.1% at 900 GeV and 1960 GeV respectively. They are an indication of non-exclusive background, probably 4-track events with two missed tracks, either below the p_T -threshold, in a calorimeter crack or very forward. We show them in Fig. 26. We expect there to be a similar number of $Q = 0$ events with missed tracks, but we do not subtract them as there is no reason for the mass spectra to be the same as the $Q = 2$ events.

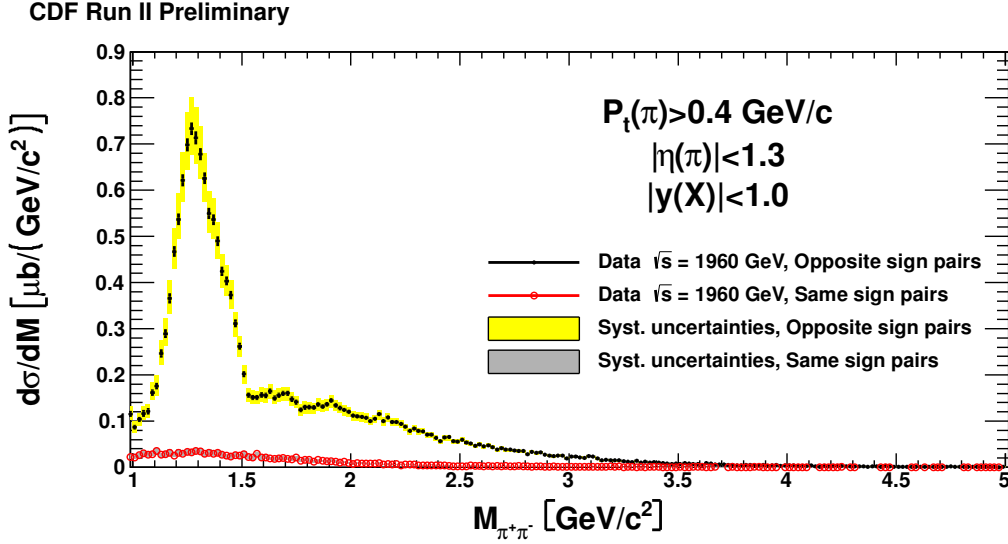


FIG. 26. Invariant mass distribution of two particles assuming pion masses - corrected for acceptance, for $\sqrt{s} = 1960 \text{ GeV}$ for oppositely-charged particles - black and pairs of particles with the same sign - red.

X. SUMMARY AND DISCUSSION

We have analysed a large sample of exclusive h^+h^- events at both $\sqrt{s} = 900$ and 1960 GeV (much larger than in other experiments with $\sqrt{s} > 30 \text{ GeV}$), nearly all $\pi^+\pi^-$, that show several resonance features. We calculated the acceptance and studied the systematic uncertainties in the M, P_t plane. We estimated the K^+K^- background to be at most 4%. We have carried out a partial wave analysis and the data are consistent with only S-wave ($J = 0$) up to about $1.5 \text{ GeV}/c^2$, but must have (at 99% C.L.) higher waves above that mass. We cannot distinguish between $J = 2$ and $J > 2$ waves, mostly because of the limited angular coverage in the forward region.

The data presented have $1.0 \text{ GeV} < M(\pi^+\pi^-) < 5 \text{ GeV}$. Between 1.0 and 1.5 GeV there is a large enhancement, initially assumed to be both $f_2(1270)$ and $f_0(1370)$ mesons. However the partial wave analysis shows only isotropic decays up to 1500 MeV , so if the dominant peak at 1270 MeV is indeed the $f_2(1270)$ it is unpolarized. At 1500 MeV the cross section shows a “break” (almost a dip) and at the same mass the mean P_t abruptly increases. A small dip has been observed there in other experiments. It requires a theoretical interpretation (it could be an effect of the opening $\rho\rho$ threshold).

ACKNOWLEDGMENTS

We thank the Fermilab staff and the technical staffs of the participating institutions for their vital contributions. This work was supported by the U.S. Department of Energy and National Science Foundation; the Italian Istituto Nazionale di Fisica Nucleare; the Ministry of Education, Culture, Sports, Science and Technology of Japan; the Natural Sciences and Engineering Research Council of Canada; the National Science Council of the Republic of China; the Swiss National Science Foundation; the A.P. Sloan Foundation; the Bundesministerium fuer Bildung und Forschung, Germany; the Korean Science and Engineering Foundation and the Korean Research Foundation; the Particle Physics and Astronomy Research Council and the Royal Society, UK; the Russian Foundation for Basic Research; the Comision Interministerial de Ciencia y Tecnologia, Spain; and in part by the European Community's Human Potential Programme under contract HPRN-CT-20002, Probe for New Physics.

-
- [1] F. Abe, et al., Nucl. Instrum. Methods Phys. Res. A **271**, 387 (1988); D. Amidei, et al., Nucl. Instrum. Methods Phys. Res. A **350**, 73 (1994); F. Abe, et al., Phys. Rev. D **52**, 4784 (1995); P. Azzi, et al., Nucl. Instrum. Methods Phys. Res. A **360**, 137 (1995); The CDFII Detector Technical Design Report, Fermilab-Pub-96/390-E
 - [2] T. Sjostrand et al., High-Energy-Physics Event Generation with PYTHIA 6.1, Comput. Phys. Commun. **135**, 238 (2001).
 - [3] T.Aaltonen *et al.* (CDF Collaboration), Phys.Rev.Lett. **102** 242001 (2009).
 - [4] T.Akesson *et al.* Phys. Lett. **133B** 268 (1983); T.Akesson *et al.*, Nucl. Phys. **B 264**, 154 (1985)
 - [5] C.Amsler, T.Gutsche, S.Spanier and N.A.Tornqvist, Note on Scalar Mesons in K.Nakamura *et al.*, (Particle Data Group), J. Phys. G. **37** 075021 (2010)
 - [6] O.V.Teryaev, R.S.Pasechnik, and A.Szczurek, Central exclusive χ_c production, Proc. 13th Int. Conf. Blois, CERN (2009)
 - [7] M.Jacob and G.C.Witt, Annal. Phys. **7** (1959) 404.
 - [8] G.Antchev *et al.*, (TOTEM Collabotration), arXiv:1204.5689, Prog.Theor.Phys.Suppl. **193** (2012) 180